B. Sundén & J. Yuan, Int. J. Comp. Meth. and Exp. Meas., Vol. 1, No. 4 (2013) 440–455

EVALUATION OF MODELS OF THE EFFECTIVE THERMAL CONDUCTIVITY OF POROUS MATERIALS RELEVANT TO FUEL CELL ELECTRODES

B. SUNDÉN & J. YUAN
Department of Energy Sciences, Lund University, Lund, Sweden.

ABSTRACT

Small scale solid particles with fluid-filled pores are applied in various porous structures in energy systems, such as fuel cells, for the objectives to enhance the catalytic reaction activities and improve the fuel utilization efficiency or/and reduce the pollutants. In addition to the catalytic reactions, heat transfer processes in fuel cell porous electrodes are strongly affected by the small scale and complex porous structures. In this paper, the thermal energy equation commonly used for continuum models at porous-averaging level is highlighted, with the purpose to provide a general overview of the validity and limiting conditions for its application. Models for effective thermal conductivity are reviewed and discussed. It is found that both the rarefaction and tortuosity effects on reduction of effective thermal conductivity may be significant, and these should be evaluated based on detailed information of operating parameters, pore size distributions and topologic structures. Comments and suggestions are presented for the better understanding and implementation of the continuum heat transfer models for fuel cell electrodes.

Keywords: Catalytic reaction, effective thermal conductivity, heat transfer, Knudsen number, modeling, multi-phase flow.

1 INTRODUCTION

Composite materials are often considered as better innovative solutions in many applications for the objective to improve and create more suitable products. Metals are gradually substituted by composite materials in, e.g. airplane structures, based on great advantages of mechanical properties. However, some drawbacks concerning heat transfer may appear, because the composite materials are usually thermal insulators compared to metals [1, 2].

High performance, low cost and high reliability are considered as the major challenges for fuel cells to compete with other well-developed power generating devices, such as internal combustion engines, gas turbines, etc. However, most research interests have focused on fuel cell new material development, processing and manufacturing techniques for specific systems, and various industries now focus on fuel cell design and optimization for better performance, improved durability, cost reduction and better cold-start characteristics, and system studies including hybrid or integrated fuel cell systems. More attention has been placed on detailed analysis and modeling of transport processes and reactions in fuel cell functional materials, components and unit cells. During recent years, one of the new trends is to apply micro or even nano-size particles in multi-functional porous materials, for the objectives to improve the fuel utilization efficiency or/and reduce the pollutants exhausted from fuel cells and batteries [3]. Various heat transfer processes appearing in heterogeneously distributed pores and solid matrices are strongly coupled with catalytic reactions and charge (proton/ions and electrons) transfer, e.g. in proton exchange membrane fuel cells (PEMFCs) and solid oxide fuel cells (SOFCs) [4–11].

In addition to the complex porous structures, rarefaction of the fluid flow and mass transfer at small scales has a significant effect on heat transfer. The Knudsen number, Kn, based on

ISSN: 2046-0546 (paper format), ISSN: 2046-0554 (online), http://journals.witpress.com
DOI: 10.2495/CMEM-V1-N4-440-455

the ratio of average distance between gas collisions (or the mean free path) and the pore/particle size has such a value that the flow and heat transfer processes fall into the temperature jump or transition regions. The interactions between the fluid and solid walls within the small scale and porous structures are strong and should be taken into account. The macroscopic transport model [such as computational fluid dynamics (CFD)] have been extensively developed, based on the volume-averaging method and treating the porous structure as a black box or as a macrohomogeneous porous region (uniformly distributed spheres or agglomerates) [3, 12–14]. With specified boundary conditions, the governing differential equations can be properly discretized on a computational grid using standard CFD techniques, such as the finite difference method, finite element method or finite volume method [15, 16]. This approach leads to a much simpler mathematical modeling procedure and correspondingly less numerical efforts. However, this methodology is developed on the basis of the so-called continuum theory, and the significant challenge is how to capture the effects of both rarefaction (small particle/pore size) and structural morphology of the porous electrodes/catalyst layers (CLs), and how to take into account effects of the interactions at the interfaces between the fluid and solid surfaces.

As pointed out in [11, 17], it is true that there are only a few experimental studies dealing with heat transfer in small scale (micrometer order) channels [17] or porous materials with moderate pore sizes and simple structures [11], and very rare for cases relevant for fuel cells. This concern has resulted in development of very detailed CFD-based models with several assumptions involved to simplify the highly reactive environment and complex nature of transport processes and reactions. For instance, an assumption is local thermal equilibrium (LTE), i.e. the gas-phase species and solid matrix within the porous electrodes are assumed to have locally the same temperature. A survey of the relevant literature indicates that most of the current fuel cell models make this assumption with marginal or no justification, see [18, 19]. In the porous electrodes in fuel cells the presence of volumetric heat generation/sink in the active sites (due to the reactions and ohmic heating effects), very low Reynolds number flow, and large difference in thermal conductivities of the solid matrix and the fluid phase may result in violation of the LTE assumption.

In summary, there are obvious needs to evaluate and highlight the critical issues on the continuum model for heat transfer modeling and analysis, with focus on how to capture the effects of the small-scale (nano-/micrometers) pores/particles and the heterogeneous porous structures. In this paper, the effective thermal conductivity being used in continuum models at the porous-averaging level is evaluated and compared with experimental data and results from microscopic approaches. The evaluation and discussion of the effective thermal conductivity models are also extended to cover the multi-functional porous materials in other applications, to identify the useful pathways to improve the fuel cell heat transfer modeling.

2 MICRO- AND NANO-SCALE POROUS MATERIALS AND HEAT TRANSFER PHENOMENA IN FUEL CELLS

In fuel cells, the composite porous electrodes facilitate the simultaneous transport of electrons, protons, and reactants/products, as well as the reactions at the so-called triple-phase boundaries (TPBs) in the electrode active region [8]. For instance, oxygen in the pores must dissolve in the Nafion and then diffuse to the TPBs in PEMFCs. More recently, with the rapid development of nano science and technology, the incorporation of nano-structured catalysts into the CLs has been proven highly successful in increasing the sites of the active TPBs and catalyst activity, thus leading to significant improvements in performance and the utilization

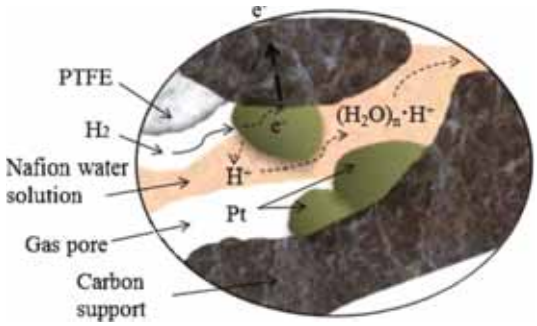

Figure 1: Schematic illustration of the anode catalyst layer (CL) in PEMFCs.

of precious-metal (Pt) catalysts. In addition to pore diameter, or particle size, there are other characteristics of the transport paths, such as porosity and tortuosity, affecting the fluid flow, heat transfer and charge transport in the porous structures.

Figure 1 shows Pt particles (with sizes of around 2–4 nm) dispersed on high surface area carbon supports and the impregnation with Nafion ionomer and polytetrafluoroethylene (PTFE, increasing the hydrophobic level to expel liquid water). Carbon particles (10–20 nm) aggregate and form agglomerates, and there are primary pores (<10 nm) existing inside the agglomerates (not shown), while the secondary pores with sizes between 10 and 50 nm build the open spaces between agglomerates. By this way, the catalyst loading can be reduced significantly.

The porous material is often modeled as homogeneous at the macroscopic scale with effective transport properties that account for the heterogeneities of the materials at the microscopic level. The Knudsen number is a dimensionless number that accounts for the effect of pore confinement on the transport processes. It is defined as the ratio of the mean free path λ to a characteristic length d of the pores:

$$\mathrm{Kn} = \frac{\lambda}{d} \tag{1}$$

$$\lambda = \frac{k_B T}{p\sqrt{2}\pi d_g^2} \tag{2}$$

where p is the fluid pressure, d_g the effective diameter of a fluid molecule, k_B the Boltzmann constant (1.3807×10^{-23} J/K), T the temperature of the fluid. The effective molecular diameters can be estimated using the appropriate covalent and van der Waals radii, while the characteristic length d should be evaluated based on the pore size or chord length distribution [11, 20]. It is clear that the operating parameters, such as pressure and temperature, are significant for the Knudsen number, and the analysis should be performed at practical operating conditions. The smaller the pores, the more frequent the collisions with the solid surfaces. In the limiting case, where the characteristic size of the pores is much smaller than the mean free path of the fluid molecules, heat transfer is entirely governed by molecule-solid collision and differs significantly from the case when the characteristic size is large, i.e. $\mathrm{Kn} \to 0$. In general, the transport processes can be divided into continuum regime ($\mathrm{Kn} < 0.001$), temperature jump regime ($0.001 < \mathrm{Kn} < 0.1$), transition regime ($0.1 < \mathrm{Kn} < 10$) and the Knudsen regime

Table 1: Typical Knudsen number and heat transfer regime in SOFC and PEMFC electrodes.

Operating conditions	Mean free path (nm)	Characteristic length (nm)	Kn	Flow and heat transfer regime	Remark
850°C/1atm	372 (O_2)	250	1.5	Transition	SOFC cathode [20]
80°C/1atm	82 (air)	10	8.2	Transition	PEMFC CL [17]
80°C/1atm	85 (H_2),41 (O_2), 51 (H_2O)	10–1000	0.04–8.5	temperature jump or transition	PEMFC micro diffusion layer [11]

(Kn > 10) [11, 17, 20]. The ranges of the Knudsen numbers for typical SOFC and PEMFC electrodes are shown in Table 1.

As revealed in Table 1, the Knudsen numbers for the fuel cell electrodes and CLs are typically in the range from the temperature jump regime to the transition regime, depending on the cell operating parameters and the scale of the pores/particles. The macroscopic continuum models at the porous-averaging level for the homogeneous porous electrodes may not be directly applied, i.e. both the rarefaction (by the small scales) and the tortuousity effects (by the complex and heterogeneous structures) on the heat transfer should be taken into account by, e.g. the effective thermal conductivity.

3 EFFECTIVE THERMAL CONDUCTIVITY AND MODELS

At the steady-state heat transfer condition, the heat transfer equation is in most cases written as:

$$(\rho c)_{\text{eff}}\,\mathbf{v}\nabla T = \nabla(k_{\text{eff}}\,\nabla T) + \dot{q} \tag{3}$$

Equation (3) is the common LTE energy equation formulated for the porous-averaging level continuum models in the open literature. $(\rho c)_{eff}$ is the effective volumetric heat capacity, k_{eff} the effective thermal conductivity, T temperature, $\dot{q}$ the heat generation and **v** the flow velocity vector.

Based on a solution for a periodic cell selected from a multi-layer, two-component composite material, the effective thermal conductivity tensor was developed in [1] by the asymptotic expansion method, which was further applied to evaluate the edge effects occurring in the vicinity of the boundaries due to the loss of periodicity. For an alumina-zirconia composite ceramic, the sigmoidal average method was applied to evaluate the effective thermal conductivity in the whole range of volume fractions, from pure alumina to pure zirconia. It was found that the experimental data are below the sigmoidal average ($k_{\text{eff}} = \phi^{+}k^{+} + (1-\phi^{+})k^{-}$, where ϕ^{+} is the volume fraction of the high-conductivity phase), which may be due to the grain size effects [2].

It should be noted that the effective thermal conductivity based on a parallel layer arrangement of the conduction, $k_{\text{eff}} = \varepsilon k_f + (1-\varepsilon)k_s$, has been often used [21, 22]. However, it is not true as discussed below, because this value is actually the maximum bound among all possible structures of the composite porous materials.

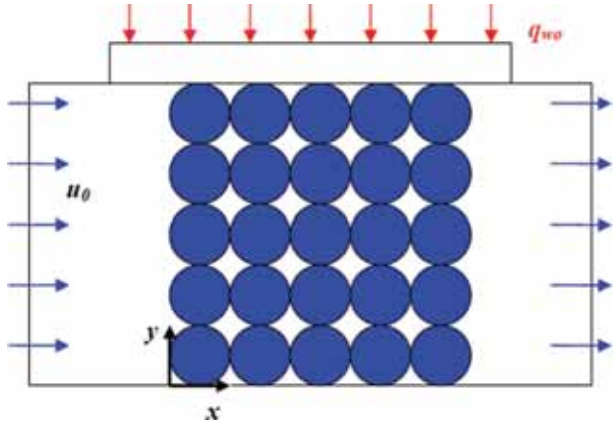

Figure 2: A simplified porous medium with 5×5 homogeneous, uniform-size solid particles.

In [23], the effective thermal conductivity k_{eff} of the porous media shown in Fig. 2 was evaluated based on the predicted temperature difference between the top and the bottom walls, and the known heat flux on the top wall by Fourier's law. The findings were compared with the values calculated from the correlation [eqn (4)], proposed in [24], with good agreement:

$$\frac{k_{\text{eff}}}{k_f} = (1-\sqrt{1-\varepsilon}) + \frac{2\sqrt{1-\varepsilon}}{1-\sigma B}\left[\frac{(1-\sigma)B}{(1-\sigma B)^2}\ln(\frac{1}{\sigma B}) - \frac{B+1}{2} - \frac{B-1}{1-\sigma B}\right] \tag{4}$$

where $B = 1.25\left[(1-\varepsilon)/\varepsilon\right]^{10/9}$, $\sigma = k_f / k_s$.

In another study, the effective thermal conductivity was, in a similar way based on the pore-level dimensionless temperature distribution, evaluated by the one-equation average model describing the conduction heat transfer in the porous media [25]:

$$k_{\text{eff}} = l\frac{-\int A_s k_s \nabla T_s \cdot \hat{\mathbf{n}} \mathrm{d}A_s - \int A_f k_f \nabla T_f \cdot \hat{\mathbf{n}} \mathrm{d}A_f}{(A_s + A_f)(T_1 - T_2)} \tag{5}$$

where T_1 and T_2 are the temperatures at the top and bottom walls, respectively, l is the length. The obtained effective conductivity is presented as a function of the solid and fluid conductivities, and this value was compared with the extreme ones from parallel and serial structures at the same porosity. The parallel structure assumes that the heat can be conducted by the solid particles and the open voids in a parallel way, while the serial structure conducts heat in the serial manner. It is found that both assumptions give maximum and minimum possible effective conductivities, respectively, and when the difference between the solid and fluid conductivities is big, the effective conductivity differs much more from either assumption. The predicted k_{eff}/k_s was further correlated by the linear combination of thermal conductivities of parallel and serial slabs:

$$\frac{k_{\text{eff}}}{k_s} = e_1 \frac{k_f / k_s}{\varepsilon(1-k_f/k_s) + k_f/k_s} + e_2(\varepsilon\frac{k_f}{k_s} + 1 - \varepsilon) \tag{6}$$

The first part of the right hand side denotes the contribution of the parallel assumption and the second one the serial. In eqn (6), $e_1 = 0.753$ and $e_2 = 0.267$, both are strongly dependent on the morphology and microstructure of the porous media [25].

The fluid flow and heat transfer were simulated by solving the governing equations and boundary conditions, assuming a no-slip interface condition at the solid–fluid interfaces, i.e. continuity in temperature and heat flux being imposed at the interfaces. Based on the predicted temperature distribution, the effective thermal conductivity was estimated for the case of air and water as the saturated fluid, as shown in Table 2. The thermal conductivity of the solid particles and the fluid phase are: $k_{\text{solid}} = 387.5$ W/m K, $k_{\text{water}} = 0.613$ W/m K and $k_{\text{air}} = 0.0265$ W/m K, respectively. It is found from Table 2 that, with the same porosity about 0.6, the effective values for the air- and water-saturated cases are rather close to each other for a specific sample, even if the water conductivity is 23 times higher than that of air. This was claimed to be attributed to the small void spaces distributed within the solid particles, particularly when the particle size is small (i.e. 47–75 μm) [26].

In contrast to other porous media like metal foams, the effective conductivity for the sintered solid particles with different particle size is much different despite the similar porosity in the porous samples. To evaluate the sintering effect, an average necking ratio was employed to characterize the amount of sintering, in terms of inter-particle contact area per unit volume:

$$Nr = \frac{A_{neck}}{V}, A_{neck} = \frac{A_s - A_{sf}}{2} \tag{7}$$

where A_{sf} is the solid–fluid interfacial area, A_s the total surface area of all the individual particles, V the total volume of solid and fluid. The necking ratio was presented in Table 2 as well, and it is clear that the most conductive porous sample has the highest necking ratio ($Nr = 1.93$ for the sample with the smallest particle size) and vice versa [26]. In comparison with other models, e.g. the Maxwell–Eucken (ME) model and the effective medium theory (EMT) model, it was pointed out that the EMT model in eqn (8), by assuming the solid particles and pores to be randomly dispersed, is better-suited for describing the effective conductivity of the sintered samples:

$$k_{\text{eff}} = \frac{1}{4}\{(3\varepsilon - 1)k_f + [3(1-\varepsilon) - 1]k_s + \sqrt{[(3\varepsilon - 1)k_f + (3(1-\varepsilon) - 1)k_s]^2 + 8k_f k_s}\} \tag{8}$$

As pointed out in [27], many of the models available in the literature are either purely empirical or theoretically based but highly specific to a given porous material, and there is no

Table 2: Predicted effective thermal conductivity k_{eff} at $k_{\text{solid}} = 387.5$, $k_{\text{water}} = 0.613$ and $k_{\text{air}} = 0.0265$ W/m K, respectively [26].

Particle size	k_{eff} (air as fluid), W/(m K)	k_{eff} (water as fluid), W/(m K)	Necking ratio, mm^{-1}
45–75 μm	53.96	55.66	1.93
106–150 μm	28.46	35.49	1.43
250–355 μm	13.83	17.91	1.06

single model or prediction procedure for the effective thermal conductivity which has found universal applicability. As proposed in [27], 'external porosity' material refers to granular or particulate type material, where the void volume is occupied by either liquid or gaseous components. 'Internal porosity' material has a continuous solid matrix that contains pores/bubbles, which may be isolated or interconnected. The effective thermal conductivity bounds, only depending on the component conductivities and volume fractions, may be defined if heat conduction is the only mechanism of heat transfer involved [26–29].

In modeling the effective thermal conductivity, the physical structure of the porous materials are often assumed as layers of the components (phases) aligned either perpendicular or parallel to the heat flow, as shown in Fig. 3a and b, respectively. As mentioned previously, the series and parallel models serve as the lowest and highest bounds, respectively, for all the heterogeneous materials (sometimes referred to as the Wiener bounds):

$$\text{Series model (the lowest bound): } k_{\text{eff}} = \frac{1}{(1-\varepsilon)/k_s + \varepsilon/k_f} \tag{9}$$

$$\text{Parallel model (the highest bound): } k_{\text{eff}} = (1-\varepsilon)k_s + \varepsilon k_f \tag{10}$$

For the objective to narrow the limitations, Hashin and Shtrikman [29] proposed effective conductivities which always lie within the Series-Parallel bounds. These narrowest bounds are mathematically equivalent to the well-known ME models, which assumed the inclusion of the dispersed component (whether particles or fluid). For a two-component material, two forms of the ME model appear depending on which of the components forms the continuous phase, as shown in Fig. 3c and d. For the case in Fig. 3c, the black (k_1) refers to the continuous phase, and the effective conductivity is as follows:

$$k_{\text{eff}} = k_1 \frac{2k_1 + k_2 - 2(k_1 - k_2)\varepsilon}{2k_1 + k_2 + (k_1 - k_2)\varepsilon}$$

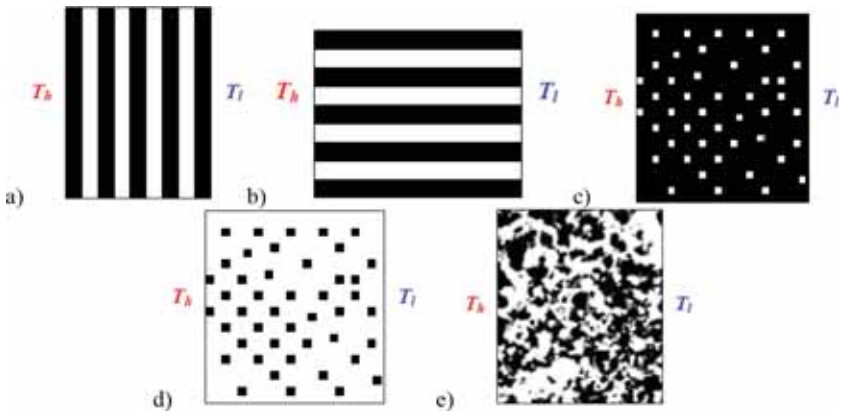

Figure 3: Structure schematic of: (a) parallel model, (b) series model, (c) Maxwell–Eucken 1 model (black = continuous phase, white = dispersed phase), (d) Maxwell–Eucken 2 model (black = dispersed phase, white = continuous phase) and (e) random model.

If the solid matrix is the continuous phase, i.e. $k_s = k_1$ and $k_f = k_2$, the above equation is formulated in a general way:

$$\text{ME1}: k_{\text{eff}} = k_s \frac{2k_s + k_f - 2(k_s - k_f)\varepsilon}{2k_s + k_f + (k_s - k_f)\varepsilon} \tag{11}$$

For the case shown in Fig. 3d, the solid particles are dispersed in a continuous fluid, and the effective conductivity is evaluated as:

$$\text{ME2}: k_{\text{eff}} = k_f \frac{2k_f + k_s - 2(k_f - k_s)(1-\varepsilon)}{2k_f + k_s + (k_f - k_s)(1-\varepsilon)} \tag{12}$$

It should be noted that, in the ME models, an assumption was that the inclusion of the dispersed component did not come into contact with neighboring inclusions [29].

It is a fact that the EMT model considers a porous material with heterogeneously distributed components, i.e. neither component is necessarily continuous or dispersed. Each component may form continuous heat transfer pathways, based on the volume fractions and local structures (Fig. 3e). Compared with the ME models, the EMT model, eqn (8), considers the effect of local distortion of complex heat transfer pathways on the temperature distribution [27]. Figure 4 compares the bounds of the effective conductivity predicted by various models for two-component porous materials at a condition of $k_s/k_f = 20$. The Maxwell models, representing the ME models, give values well between those by the series and the parallel models (the lowest and the highest possible values).

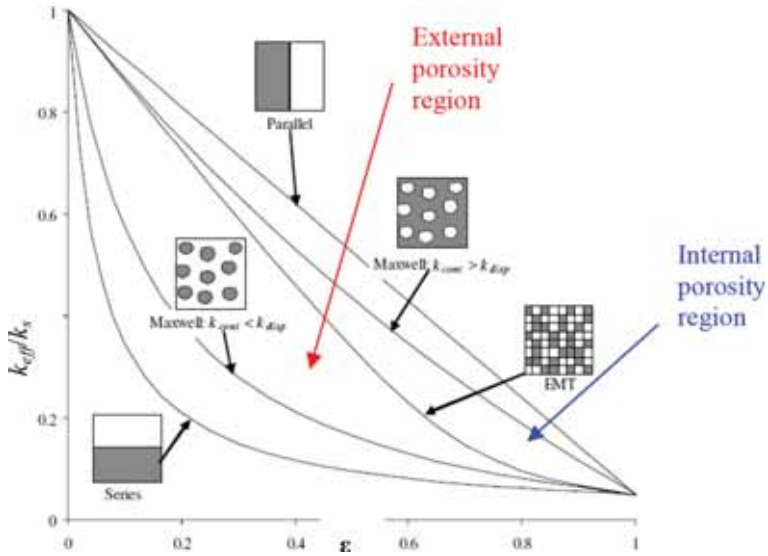

Figure 4: Effective conductivity bounds with schematic representations of the assumed structure at $k_s/k_f = 20$. k_{cont} refers to the conductivity of the continued component, while k_{disp} is the one of the dispersed phase [27]. (Permission obtained from Elsevier).

As shown in Fig. 4, the EMT bound is close to the ME1 bound when the porosity is small, while it approaches to the one by ME2 when the porosity is big, which indicates an S-shaped behavior. It is found that the effective conductivity of external porosity materials (the fluid is the continuous phase) will be in the region bounded by the ME2 (lower limit) and EMT (upper limit) models, while the effective values of internal porosity materials (the solid is the continuous phase) are bounded by the EMT (lower limit) and the ME 1 (upper limit) models [27].

It is also clear, as presented in Fig. 4, that the external porosity region is larger than the internal porosity region, which is true for any value of k_s/k_f. This means that there is inherently more uncertainty in the estimation of the thermal conductivity of the external porosity materials. However, for low volume fractions of the dispersed phase (i.e. $\varepsilon < 0.2$ for the external porosity materials or $\varepsilon > 0.8$ for the internal porosity materials), the predictions of the Maxwell and EMT models are nearly identical [26, 27].

In [30], the effective thermal conductivity of the silica grain network constituting the porous structure, as shown in Fig. 5a, was evaluated based on the structure parameters (density, solid conductivity, grain diameter, contact area between grains, etc.) and operating conditions (e.g. at atmospheric pressure and a primary vacuum, $p = 1000$ Pa). It was found in Fig. 5b that, for relatively high porosities (i.e. low densities on the horizontal axis), the effective thermal conductivity is even smaller than the one of free air ($k_{air} = 0.0257$ W/m K), particularly for the case of low partial pressure ($p = 1000$ Pa) and the small silica grain diameter ($d_{grain} = 5$ nm). It is also interesting to point out that the effective conductivity can be as small as 0.03 W/(m K) (a good thermal insulation), when the silica particle size is about 10 nm even at atmospheric pressure condition.

In an experimental study in [31], the Knudsen number effect on the thermal conductivity of gas filling in zeolite powders was evaluated as:

$$k_{f,Kn} = \frac{k_f}{1 + 2\beta Kn} \tag{13}$$

in which β is a constant considering the accommodation coefficient, i.e. the effectiveness of heat transfer between the fluid molecules and the solid walls. For example, $\beta = 1.5$ was suggested in [31].

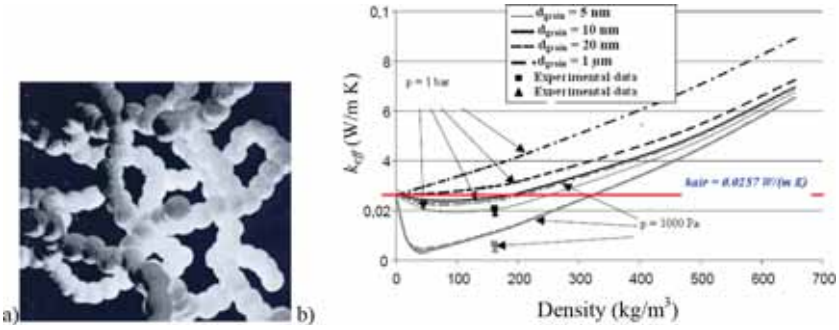

Figure 5: (a) Representation of the random structure of nanometric porous silica, and (b) effective thermal conductivity predicted for various densities [30]. $k_{air} = 0.0257$ W/m K and $k_{silica} = 1.4$ W/(m K).

Table 3: Effective thermal conductivity in fuel cell electrodes.

Case	Kn	$k_{f,Kn}$	k_s	Volume Fraction (%)	Parallel	Series	ME1	ME2	EMT	Exp. Data	Remarks
SOFC anode	1	0.21	2(YSZ)/ 50(Ni)	41(pore)/ 33(YSZ)/ 26(Ni)	13.73	0.076	11.45	1.06	9.19	4.23/ 4.54/ 3.27	*x*/*y*/*z* direction [32]
PEMFC GDL	0.04	0.017	129(C)/ 11.7 (PTFE)	71(pore)/ 22(C)/ 7(PTFE)	29.91	0.012	21.56	0.04	0.15	0.3	[33]

Recently the effective thermal conductivity has been experimentally measured for specific fuel cell electrodes, e.g. for an SOFC anode in [32] and for PEMFC gas diffusion layers (GDLs) in [33, 34]. Based on a focused ion beam-scanning electron microscope, the three-dimensional microstructure of an SOFC anode was reconstructed and characterized to evaluate the effective parameters and the tortuosity of the solid phases in [32]. The volume fractions calculated from 3D data were: 41% for the pores, 33% for the 8YSZ and 26% for the Ni (roughly 40vol% for Ni and 60vol% for 8YSZ). The mean free path of hydrogen molecules in the anode was close to 900 nm, which is comparable to the characteristic size of the anode pores [32], i.e. Kn ~ 1. The fluid (hydrogen) thermal conductivity (k_{H2} = 0.48 W/m K) is corrected by eqn (13) to consider the rarefaction effect, as shown in Table 3. The effective thermal conductivity bounds by different models are calculated and presented in Table 3 as well. It is clear that the experimentally measured thermal conductivities (4.23/4.54/3.27 W/m K in *x*, *y*, *z* directions, respectively) are well falling in the external porosity region in Fig. 4, which is bounded by the ME2 model (1.06 W/m K) and the EMT model (9.19 W/m K). It should be noted that the variation of the measured data in *x*, *y*, *z* directions were due to dissimilar Ni concentrations, as notified in [32].

The effects of PTFE concentration coated on the carbon fibers and compression on the effective thermal conductivity and thermal contact resistance were evaluated for the through- and in-planes of the GDLs used in PEMFCs [33–36]. Based on the samples used in [33], the diameters of the pores in the Toray carbon fiber d_p were between 16×10^{-9} and 80×10^{-6} m. A typical Knudsen number Kn = 0.04 (when $d_p = 1 \times 10^{-6}$ m) is used in this study for the correction of the fluid (air) thermal conductivity. The corresponding bounds by the different models are calculated and presented in Table 3. It is clear that the measured effective thermal conductivity (0.3 W/m K) falls in the internal porosity materials bounded by the ME1 and the EMT models, i.e. 21.56 and 0.15 W/m K, respectively, which are much narrower than the ones by the series and parallel models (29.91 and 0.012 W/m K, respectively).

For the porous materials with complex structures, there are some approaches commonly used to combine the basic structural models using empirical weighting or other functions, such as the so-called Krischer model [27, 37] or the one using simple combinatory rules [28]. In general, the thermal conductivities of any two-component material must lie between the Wiener bounds and its thermal conductivity might be estimated by a mixture of series and parallel models:

$$k_{\text{eff}} = \frac{1}{f / k_{\text{series}} + (1-f) / k_{\text{parallel}}} \tag{14}$$

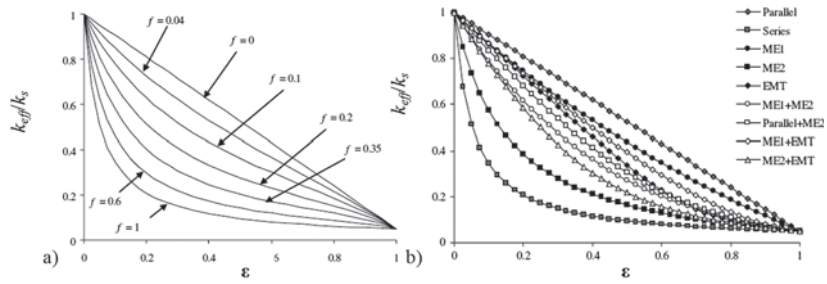

Figure 6: Effective thermal conductivity predicted for a two-component material by: (a) a weighting function approach, and (b) a simple combinatory rule method of binary-structure models. ME1 and ME2 refer to the Maxwell–Eucken models 1 and 2, respectively, EMT represents effective medium theory model. k_s/k_f = 20 [28]. (Permission obtained from Elsevier).

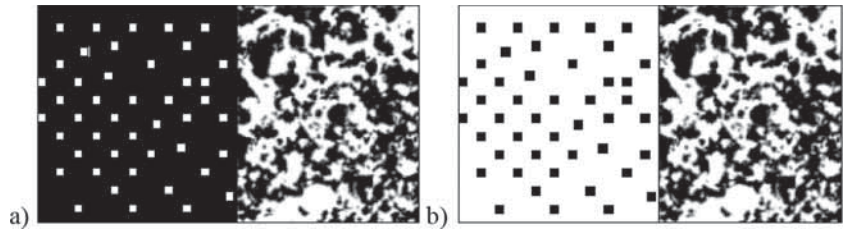

Figure 7: Schematic representations of two-component (solid and fluid) materials as uniform mixtures of two basic structure models: (a) ME1 + EMT and (b) ME2 + EMT. Black represents the solid phase material, and white is for the fluid.

where k_{series} and k_{parallel} are the effective conductivities by the series and parallel model, respectively, while f (between 0 and 1) is the weighted geometric or arithmetic means. In a similar way, this approach may be extended using the narrower bounds, such as those by the ME and EMT models, for the external and internal porosity materials [27]. However, the values of the weighting parameters are not easily determined mechanistically from information about the physical structures. Based on the structure volume fraction (distinct from component or phase material volume fraction), a combinatory rule was applied for a material with known components and specified structures by combining the basic bound models (as shown in Figs 4 and 5). When equal structure volumes and equal structure effective thermal conductivities are assumed, the combinatory rule is the simplest [28]. For a two-component porous material, Fig. 6a shows the effective conductivity for different values of f based on the weighting factor approach, while Fig. 6b shows the five basic conductivity bounds, together with the predictions by the simple combinatory rule method applied for binary-structure porous materials.

Two of the possible 10 theoretical two-component material structure models with an equal mixture of two of five fundamental structure models are highlighted in Fig. 7. In Fig. 7a, the

left half of the volume has the ME structure with component 1 (black) as the continuous phase (ME1), and the right half of the volume has the MET structure. While the left half of the volume in Fig. 7b changes to ME2, i.e. the component 2 (white) is the continuous phase instead. The ME1+MET model in Fig. 7a provides a logical intermediate structure between these two extremes that may be more accurate for an internal porosity material that has neither a true Maxwell structure nor a true EMT structure. This combinatory rule approach was further extended for ten ternary, five quaternary and one five-structure models for two-component porous materials with high degree variability in terms of the local structures. As claimed in [28], the procedure using simple combinatory rules to evaluate the effective thermal conductivities of complex materials is only dependent on volume fractions and thermal conductivities of the component materials, and not on any empirical parameter.

For simplicity, the sigmoidal average of the upper and lower bounds, originally developed for isotropic two-component composites, may be applied for the estimation of the effective thermal conductivity [2]:

$$k_{\text{eff}} = (1-\varepsilon)k_{\text{upper}} + \varepsilon k_{\text{lower}} \tag{15}$$

in which k_{upper} is the effective thermal conductivity bound by, e.g. the EM1 and the EM2 models, respectively. As long as the ratio of the solid and fluid thermal conductivities is about one order of magnitude or higher, such as the case involving the solid particles and the fluid-filled pores in the fuel cell electrodes, the lower bound will approach a very small value. The sigmoidal average then reduces to the simplest one, i.e. only the thermal conductivities of the solid materials are involved, as written below [2]:

$$k_{\text{eff}} = \frac{(1-\varepsilon)^2}{1+\varepsilon/2} k_s \tag{16}$$

In addition, there are several nonlinear relations for predicting the effective conductivity of the porous materials, such as the power-low relation (not shown) and the exponential relation:

$$k_{\text{eff}} = \exp\left(\frac{-\frac{3}{2}\varepsilon}{1-\varepsilon}\right) k_s \tag{17}$$

By using the above relations, the effective thermal conductivity of the SOFC anode (see Table 3) is predicted to be 6.68 and 8.16 W/(m K) by eqns (16) and (17), respectively, while for PEMFC GDL (see Table 3), the predictions are 6.24 and 2.55 W/(m K), respectively. It is revealed that the sigmoidal average in eqn (16) gives a better estimation for the SOFC anode (compared to the experimental data in Table 3), in which the porosity, 0.41, is smaller than 0.55. For PEMFC GDL, however, its porosity is 0.71 (bigger than 0.55), the exponential relation in eqn (17) predicts a better value. A similar finding was also indicated in [2]. In other words, different relation should be selected for the evaluation of the effective thermal conductivity based on the specific porous structures, such as the porosity if no other microstructure information is available. It should be noted that these estimated values are well above the experimental data, which suggests that the effects of both the heterogeneous structures (the tortuosity effects) and the interfaces between the sintered particles (the mixture phase) may be significant in reducing the thermal conductivities of the solid materials in fuel cell components.

It should be noted that this paper concerns how to calculate or estimate the effective thermal conductivity. There are studies aiming at enhancing the effective conductivity and also papers considering other thermophysical properties, e.g. [38, 39].

4 SUMMARY AND CONCLUSIONS

Small scale solid particles (the catalysts and the supporting materials) at micro-/nano-meter scales are often applied in the multi-functional porous materials, such as in the GDLs and the CLs in the fuel cells. The transport phenomena are strongly affected by the catalytic reactions, and more significantly by the small scales (rarefaction effect) and heterogeneous structures (tortuosity effect). However, both effects have attracted limited attention in fuel cell modeling societies.

It is found from the literature review in this paper that the effective thermal conductivity is, one of the significant parameters, necessary for the porous-averaging level continuum heat transfer models developed for complex porous materials. However, these studies were often limited to the simple (spherical and rectangular) shapes of the homogeneously distributed solid particles, and the size of the particles was usually very big (in the order of μm to mm). Under these conditions the Knudsen number is small enough to ignore the rarefaction effect, i.e. no-slip interface conditions could be implemented at the interfaces.

It is also true that the effective thermal conductivity applied in the porous-averaging level continuum LTE models has been based on the parallel model assumption, which only depends on the fluid and solid phase conductivities and porosity. Actually this value is the maximal possible value. It is suggested that the effective thermal conductivities of the fuel cell electrodes fall into the one of the regions bounded by one of the ME bounds and the EMT bound. For the case when the porosity is the only known parameter, the effective thermal conductivity of the porous fuel cell electrode may be estimated by the sigmoidal average (eqn (16)) or the exponential relation (eqn (17)). However, the predictions by the sigmoidal average or the exponential relation are always well above the experimental data. This suggests that further studies are required to explore and capture the effects of the tortuosity and the sintered interfaces on the reduction of the effective thermal conductivity and to find proper models.

ACKNOWLEDGMENT

The financial support from the Swedish Research Council (VR-621-2010-4581) and the European Research Council (ERC-226238-MMFCs) is gratefully acknowledged.

REFERENCES

[1] Matine, A., Boyard, N., Cartraud, P., Legrain G. & Jarny, Y., Thermal properties of composite materials: Effective conductivity tensor and edge effects. *6th European Thermal Sciences Conference*, 4–7 September 2012, France.

[2] Pabst, W. & Gregorová, E., The sigmoidal average-a powerful tool for predicting the thermal conductivity of composite ceramics. *6th European Thermal Sciences Conference*, 4–7 September 2012, France.

[3] Wang, Y., Chen, K.S., Mishler, J., Cho S.C. & Adroher, X.C., A review of polymer electrolyte membrane fuel cells: Technology, applications, and needs on fundamental research. *Applied Energy*, **88**, pp. 981–1007, 2011. doi: http://dx.doi.org/10.1016/j.apenergy.2010.09.030

[4] Mukherjee, P.P., Kang, Q. & Wang, C.Y., Pore-scale modeling of two-phase transport in polymer electrolyte fuel cells–progress and perspective. *Energy & Environmental Science,* **4**, pp. 346–369, 2011. doi: http://dx.doi.org/10.1039/b926077c

[5] Yan, Q. and Wu, J., Modeling of single catalyst particle in cathode of PEM fuel cells. *Energy Conversion and Management*, **49**, pp. 2425–2433, 2008. doi: http://dx.doi.org/10.1016/j.enconman.2008.01.021

[6] Xiao, Y., Dou, M., Yuan, J., Hou, M., Song W. & Sundén, B., Fabrication process simulation of a PEM fuel cell catalyst layer and its microscopic structure characteristics. *Journal of the Electrochemical Society*, **159**, pp. B308–B314, 2012. doi: http://dx.doi.org/10.1149/2.064203jes

[7] Xiao, Y., Yuan, J. & Sundén, B., Process Based Large Scale Molecular Dynamic Simulation of a Fuel Cell Catalyst Layer. *Journal of the Electrochemical Society*, **159(3)** pp. B251–B258, 2012. doi: http://dx.doi.org/10.1149/2.028203jes

[8] Andreaus, B. & Eikerling, M., Catalyst layer operation in PEM fuel cells: From structural pictures to tractable models. *Device and Materials Modeling in PEM Fuel Cells*, eds. S.J. Paddison, & K.S. Promislow, Springer Science: New York, NY, USA, pp. 41–90, 2009.

[9] Moore, K.L. & Reeves, K.S., Microstructural characterization of PEM fuel cell MEAs. *DOE Hydrogen Program Annual Merit Review Proceedings*, Arlington, VA, USA, May 23–26, 2005.

[10] Xiao, Y., Yuan, J. & Sundén, B., Review on the properties of nano-/micro- structures in the catalyst layer of PEMFC. *ASME Journal of Fuel Cell Science and Technology*, **8**, pp. 1–13, 2011.

[11] Jiao K. & Li, X., Water transport in polymer electrolyte membrane fuel cells. *Progress in Energy and Combustion Science*, **37**, pp. 221–291, 2011. doi: http://dx.doi.org/10.1016/j.pecs.2010.06.002

[12] Yuan, J. & Sundén, B., Two-Phase flow analysis in a cathode duct of PEFCs. *Electrochimica Acta*, **50**, pp. 677–683, 2004. doi: http://dx.doi.org/10.1016/j.electacta.2004.01.118

[13] Yuan, J., Sundén, B., Hou, M. & Zhang, H., Three-Dimensional analysis of two-phase flow and its effects on the cell performance of PEMFCs. *Numerical Heat Transfer (Part A)*, **46**, pp. 669–694, 2004. doi: http://dx.doi.org/10.1016/j.electacta.2004.01.118

[14] Khan, M., Sundén, B. & Yuan, J., Analysis of multi-phase transport phenomena with catalyst reactions in PEMFC-a review. *Journal of Power Sources*, **196**, pp. 7899–7916, 2011. doi: http://dx.doi.org/10.1016/j.jpowsour.2011.04.040

[15] Date, A.W., *Introduction to Computational Fluid Dynamics*, Cambridge University Press: New York, USA, 2005. doi: http://dx.doi.org/10.1017/CBO9780511808975

[16] Versteeg, H.K. & Malalasekera, W., *An Introduction to Computational Fluid Dynamics -The Finite Volume Method*, 2nd edn., Pearson Education Limited: Essex, England, 2007.

[17] Cecen, A., Wargo, E.A., Hanna, A.C., Turner, D., Kalidindi, S.R. & Kumbur, E.C., 3-D microstructure analysis of fuel cell materials: Spatial distributions of tortuosity, void size, and diffusivity. *Journal of the Electrochemical Society*, **159**, pp. B1–B9, 2012.

[18] Andersson, M., Yuan, J., Sundén, B. & Wang, W.G., LTNE Approach and Simulation for Anode-Supported SOFCs, *ASME FuelCell2009-85054*, USA, 2009. doi: http://dx.doi.org/10.1016/j.apenergy.2009.11.013

[19] Andersson, M., Yuan, J. & Sundén, B., Review on modeling development for multiscale chemical-reactions-coupled transport phenomena in SOFCs. *Applied Energy*, **87(5)**, pp. 1461–1476, 2010.

[20] Berson, A., Choi, H.W. & Pharoah, J.G., Determination of the effective gas diffusivity of a porous composite medium from the three-dimensional reconstruction of its microstructure. *Physical Review E*, **83**, p. 026310, 2011. doi: http://dx.doi.org/10.1103/PhysRevE.83.026310

[21] Ichikawa, Y. & Selvadurai, A.P.S., *Transport Phenomena in Porous Media*, Springer-Verlag Berlin Heidelberg: Berlin, Germany, 2012.
[22] Delgado, J.M.P.Q., *Heat and Mass Transfer in Porous Media*, Springer-Verlag Berlin Heidelberg: Berlin, Germany, 2012.
[23] Jiang, P.X. & Lu, X.C., Numerical simulation of fluid flow and convection heat transfer in sintered porous plate channels. *International Journal of Heat and Mass Transfer*, **49**, pp. 1685–1695, 2006. doi: http://dx.doi.org/10.1016/j.ijheatmasstransfer.2005.10.026
[24] Zehener, P., Thermal conductivity of granular materials at moderate temperatures. *Chemie Ingenieur Technik*, **42**, pp. 933–941, 1970.
[25] Haussener, S., Coray, P., Lipiński, W., Wyss, P. & Steinfeld, A., Tomography-Based heat and mass transfer characterization of reticulate porous ceramics for high-temperature processing. *ASME Journal of Heat and Mass Transfer*, **132(2)**, p. 023305-1, 2010. doi: http://dx.doi.org/10.1115/1.4000226
[26] Bodla, K.K., Murthy, J.Y. & Garimella, S.V., Direct simulation of thermal transport through sintered wick microstructures. *ASME Journal of Heat and Mass Transfer*, **134(1)**, p. 012602, 2012. doi: http://dx.doi.org/10.1115/1.4004804
[27] Carson, J.K., Lovatt, S.J., Tanner, D.J. & Cleland, A.C., Thermal conductivity bounds for isotropic, porous materials. *International Journal of Heat and Mass Transfer*, **48(11)**, pp. 2150–2158, 2005. doi: http://dx.doi.org/10.1016/j.ijheatmasstransfer.2004.12.032
[28] Wang, J., Carson, J.K., North, M.F. & Cleland, D.J., A new approach to modelling the effective thermal conductivity of heterogeneous materials. *International Journal of Heat and Mass Transfer*, **49**, pp. 3075–3083, 2006. doi: http://dx.doi.org/10.1016/j.ijheatmasstransfer.2006.02.007
[29] Hashin, Z. & Shtrikman, S., A variational approach to the theory of the effective magnetic permeability of multiphase materials. *Journal of Applied Physics*, **33**, pp. 3125– 3131, 1962. doi: http://dx.doi.org/10.1063/1.1728579
[30] Coquard, R. & Quenard, D., Modeling of Heat Transfer in Nanoporous Silica-Influence of Miosture. *8th Int. Vacuum Insulation Sym.,* 18th–19th September 2007, Würzburg, Germany.
[31] Griesinger, A., Spindler, K. & Hahne, E., Measurements and theoretical modeling of the effective thermal conductivity of zeolites. *International Journal of Heat and Mass Transfer*, **42(23)**, pp. 4363–4374, 1999. doi: http://dx.doi.org/10.1016/S0017-9310(99)00096-4
[32] Vivet, N., Chupin, S., Estrade, E., Piquero, T., Pommier, P.L., Rochais, D. & Bruneton, E., 3D microstructural characterization of a solid oxide fuel cell anode reconstructed by focused ion beam tomography. *Journal of Power Sources*, **196**, pp. 7541–7549, 2011. doi: http://dx.doi.org/10.1016/j.jpowsour.2011.03.060
[33] Nikooee, E., Karimi, G. & Li, X., Determination of the effective thermal conductivity of gas diffusion layers in polymer electrolyte membrane fuel cells: A comprehensive fractal approach. *International Journal of Energy Research*, **35**, pp. 1351–1359, 2011. doi: http://dx.doi.org/10.1002/er.1896
[34] Khandelwal, M. & Mench, M.M., Direct measurement of through-plane thermal conductivity and contact resistance in fuel cell materials. *Journal of Power Sources*, **161**, pp. 1106–1115, 2006. doi: http://dx.doi.org/10.1016/j.jpowsour.2006.06.092
[35] Sadeghi, E., Djilali, N. & Bahrami, M., A novel approach to determine the in-plane thermal conductivity of gas diffusion layers in proton exchange membrane fuel cells. *Journal of Power Sources*, **196**, pp. 3565–3571, 2011. doi: http://dx.doi.org/10.1016/j.jpowsour.2010.11.151

[36] Sadeghi, E., Djilali, N. & Bahrami, M., Effective thermal conductivity and thermal contact resistance of gas diffusion layers in proton exchange membrane fuel cells. Part 1: Effect of compressive load. *Journal of Power Sources*, **196**, pp. 246–254, 2011. doi: http://dx.doi.org/10.1016/j.jpowsour.2010.06.039

[37] Chaudhary, D.R. & Bhandari, R.C., Heat transfer through a three-phase porous medium. *Journal of Physics D* (*British Journal of Applied Physics*), **1**, pp. 815–817, 1968. doi: http://dx.doi.org/10.1088/0022-3727/1/6/418

[38] Wang, M., Kang, Q. & Pan, N., Thermal conductivity enhancement of carbon fiber composites. *Applied Thermal Engineering*, **29(2)**, pp. 418–421, 2009. doi: http://dx.doi.org/10.1016/j.applthermaleng.2008.03.004

[39] Wang, M. & Pan, N., Predictions of effective physical properties of complex multiphase materials. *Materials Science and Engineering: R: Reports*, **63(1)**, pp. 1–30, 2008. doi: http://dx.doi.org/10.1016/j.mser.2008.07.001